New development of Nanosilver manufacture using abelmoschus esculentus l. pods extract as Bioreductor by Tollen's method and anti-colon cancer ability

Ally Kasefa[1,2], Sri Puji Astuti Wahyuningsih[2], Win Darmanto[2*], Nada Syazana Zulkufli[3]

[1]Department of Medical Laboratory Technology Faculty of Health, Institute Kesehatan Rajawali, Bandung, Indonesia.
[2]Doctoral Program of Mathematics and Natural Science, Faculty of Science and Technology, University of Airlangga, Surabaya, Indonesia.
[3]Beacon Precision Diagnostics, Petaling Jaya, Sleangor, Malaysia.

Corresponding author: Win Darmanto (*Email: windarmanto@fst.unair.ac.id*)

Abstract

Nanosilver (AgNP) has many uses as a result of its unique properties, including cancer prevention. In a previous study, the Turkevich Method approach used to make AgNPs by utilizing polysaccharides from okra pods (ORPE) as a bioreductor produced AgNPs larger than 100 nm in size. The resulting anti-colon cancer effect causes necrosis and apoptosis when interacting with colon cancer cells. Necrosis can aggravate cancer by causing new inflammation. Tollen's method, which uses organic catalysts, has the potential to create superior AgNPs. Developing novel AgNPs to meet the standard size of nanodrugs for anti-colon cancer is the goal of this study. This research included a type of experimental research with the posttest nonequivalent control group design, which aims to find the effect of certain treatments under directed conditions of AgNP. PSA, zeta potential, SEM, TEM, X-ray spectroscopy, and UV-Vis spectrophotometry are used to test AgNP characteristics. Cell viability assays, apoptotic potential, and flow cytometry cell cycle analysis were used to evaluate AgNP's potential as an anti-colon cancer agent. The characteristics of AgNP-ORPE were observed: UV absorbance at ʎmax 198.93 nm, particle size 107.8 ± 25.47 nm with PDI of 0.87521 ± 0.001 mPas, zeta potential value -8.7 ± 0.15 mV, SEM showed AgNP in the form of asymmetric spheres, and TEM in the form of anisotropic appearing spherical asymmetrical with an average size of 50.85 nm. The viability test of living cells at a concentration of 0-30 μg/mL and evaluation of the potential for apoptosis was 79.68%. The IC50 value obtained was 21.43 μg/mL. In the cell cycle, the G0/G1 phase decreased (17%) lower than the control, and there was an accumulation in the G2/M phase of 11.0%. The new development of AgNP-ORPE production by Tollen's method produced anisotropic spherical asymmetries AgNPs with a size of 50.85 nm and good stability. It also had an anti-colon cancer effect by significantly reducing the proliferation of the colon cancer cell cycle in the G0/G1 phase and inducing apoptosis of the intrinsic pathway.

Keywords: Anti colon cancer, Nanosilver, Okra Raw Polysaccharide Extract, Tollen's method.

Competing Interests: The authors declare that they have no competing interests.
Authors' Contributions: All authors contributed equally to the conception and design of the study. All authors have read and agreed to the published version of the manuscript.

1. Introduction

Colon cancer is a malignancy that originates from the tissues of the large intestine, which consists of the rectum (the last small part of the large intestine before the anus) and the colon (the longest part of the large intestine) [1]. Colon cancer accounts for about 40% of cancer cases in the USA. In a country with a large population like India, the mean incidence of colon cancer (male and female) is 4.4 and 3.9 per 100,000 population, respectively. In 2020, there were cases of death from colon cancer, and this showed an increasing trend in countries with less than 40% clean living behavior, such as India, Indonesia, and Mongolia. Epidemiological studies show that the colon cancer case rate is 10%, and the colon cancer mortality rate is 9.4%, with the majority of men at high risk (WHO, 2020).

There is a determining factor in the cure of colon cancer (based on diagnosis), and several types of treatment are available depending on the stage of the disease [2]. Surgery, radiofrequency ablation, cryosurgery, chemotherapy, radiation therapy, targeted therapy, and immunotherapy are the seven treatments (which can be combined) that make up the traditional approach to treating colon cancer [2, 3]. The AJCC and National Cancer Institute's TNM (Tumor, Node, Metastasis) classification serves as the basis for the combination of employed therapeutic treatments [4]. Stage 0, Stage I, Stages II (A, B, C), Stages III (A, B, C), and Stage IV (A, B, C) are the AJCC stage groups and TNM definitions [5]. The standard of therapy for individuals with colon cancer who have localized illness has been surgical removal of the primary tumor and regional lymph nodes. Patients who receive radiation, chemotherapy, or surgery run a significant risk of complications, disability, and death [2, 5]. According to the FDA, there are sixteen medications available, twelve of which are administered intravenously and four of which are taken orally [6]. It is well recognized that conventional medications are poorly soluble [5], have non-specific targets [7], accumulate poorly in tumor cells, and are dose-dependent on healthy cells and tissues Strużyńska [8]. Zhang et al. [9] used antibodies against the epidermal growth factor receptor (EGFR-Mab), which include IMC-C255, ABX-EGF, EMD, hR3, and ICR62, to dimerize and prevent cancer. CTLA inhibitors and PD-1 & PD-L1 are immune checkpoint inhibitors that are frequently used in immunotherapy [9]. These proteins attach to the B7-1/B7-2 proteins in cancer cells, preventing T cells from killing cancer cells [9, 10]. Hematopoietic suppression, limited efficacy, immunotoxicity, and drug resistance are some of the drawbacks of using therapeutic medications [11]. Nanomedicine employing nanodrugs is a promising therapeutic [10, 12] approach that can be utilized as a diagnostic tool to address the shortcomings of these treatments.

According to earlier research conducted over the past few decades, nanoparticles have emerged as a popular trend in the hunt for novel anticancer treatments [13]. Since every nanodrug has distinct qualities, a variety of nanomaterials, including nanosilver (AgNPs), are being explored as possibilities [14]. Numerous physical and chemical techniques can be used to create AgNPs. AgNPs with a very small size and high concentration can be obtained by physical processes [15]. The two most used techniques are laser ablation and evaporation-condensation [15, 16]. These procedures involve a furnace that uses a lot of energy, takes up a lot of space, and/or takes a long time [12]. AgNPs less than 10 nm were produced via the physical production of AgNPs with AgNO3 precursor utilizing reducing agent electrical arc discharge with stability agent sodium citrate [17]. AgNPs of 2–5 nm were generated by a combination of the stability agents AOT and the reduction agent hydrazine hydrate in a photochemical AgNPs size (microemulsion) with AgNO3 precursor. Both organic and inorganic substances can be employed as reducing agents in chemical processes. Using reducing agent DMF (<25 nm), NaBH4 with stabilizing agent surfactin (3-28 nm), Trisodium citrate (30-60 nm), paraffin with stabilizing agent oleylamine (10-14 nm), dextrose with stabilizing agent PVP (22 ± 4.7 nm), glucose with stabilizing agent gluconic acid (40-80 nm), and ethylene glycol with stabilizing agent PVP (50-115 nm) were among the different particle sizes that were produced by the chemical formation of AgNPs with AgNO3 precursor [15]. Because the ingredients and processes needed to produce AgNPs are simpler and less expensive, chemical approaches are frequently chosen.

Depending on the biology of the target cells, AgNPs can cause cell death in both healthy and malignant tissues, which underpins their therapeutic potential. In the framework of creating new, efficient treatment tools in conjunction with other therapeutic approaches, current opinions regarding the potential of AgNPs in oncotherapy have recently been reviewed [18]. As a result, by causing autophagy and/or apoptosis in cancer cells, they may be employed as anticancer agents to supplement conventional treatments [8]. AgNPs' toxicity and effectiveness against different cancer types demonstrate a range of distinct impacts on cancer cell death [8]. The human prostate cancer cell line (PC-3) AgNPs-PVP diameter is 78.24 ± 0.58 nm, lysosomal breakdown takes place, and there are no apoptotic cells (Annexin-V FITC/PI). This is an example of how cancer cell death on apoptosis markers generally differs [19]. DNA fragmentation did not occur in breast cancer cells (SKBR3) with an AgNps diameter of N/A nm. AgNPs with a diameter of 10–20 nm triggered caspase 3 in the apoptotic pathway in lung epithelial carcinoma cells (A549) [8]. Apoptosis and a rise in the proteins cyt-C, p53, Bax, ASP3, CASP8, CASP9, and CASP12 occur in the colorectal cancer cell line (HT-29) with a diameter less than 100 nm [20]. Apoptosis and necrosis were observed in the colorectal cancer cell line (HCT 116), where the diameter of AgNPs with Okra Raw Polysaccharide Extract (AgNP-ORPE) was 248.52 nm, Kafesa et al. [21]. Kafesa et al. [21] observed that due to the failure of oxidative

phosphorylation and loss of ion channel regulation, the AgNP-ORPE size achieved by the Turkevich approach is not nearly optimal (less than 100 nm), which results in fresh inflammation when it interacts with cancer cells in the intrinsic pathway [21]. In order for the AgNPs produced to have an average of less than 100 nm [21], it is vital to develop the size and form of AgNP-ORPE while still using the modified ORPE in Tollen's approach.

The modified Tollens process, on the other hand, produces silver nanoparticle films (50-200 nm), silver hydrosols (20-50 nm), and AgNPs with certain morphologies by reducing Ag+ ions with various types of saccharides amid ammonia [22]. The size and shape of AgNPs were regulated in this green synthesis by varying the ammonia content and the reducing agent type. Moreover, [Ag(NH3)2]+ is reduced with glucose, galactose, maltose, lactose, and polysaccharides to create AgNPs of regulated size [22, 23]. Sodium dodecyl sulfate, polyoxyethylene sorbitane monooleate (Tween 80), and polyvinylpyrrolidone (PVP 360) [24] are some of the materials that can be utilized as stabilizing and capping agents to increase the stability of AgNPs. PVP is amorphous and can undergo crosslinking when exposed to UV light or in an alkaline environment [23, 24]. The glycol derivatives poly-N-vinyl-2-pyrrolidone (PVP) and polyethylene glycol (PEG) are often utilized materials in the synthesis of AgNPs. PVP must be included in this method's modification in order to prevent aggregated nanoparticles and stabilizers [24, 25].

In order to decrease Tollen's reagent [Ag(NH3)2]+ (aq) to AgNPs, a hybrid synthesis technique using ORPE in place of saccharide [22] is presented in this work. For the manufacture of AgNPs using ORPE and Tollen's reagent, a novel reduction technique utilizing the well-known nanosuspensions stabilizer was created in this work. As a result, a more ecologically friendly synthesis was produced, displaying traits of suitable nanoparticles. In the end, it is anticipated that this strategy will accomplish the objective of enhancing the resulting nanoparticles' replicability in terms of their size, shape, and stability. Given the distinctiveness and properties of these novel AgNPs, in vitro research using the AgNP-ORPE interaction experiment with the HCT 116 cell line is required to ascertain their anti-colon cancer properties.

2. Materials and Methods

2.1. Materials

Silver nitrate (Sigma Aldrich, *ReagentPlus®*, $\geq$ 99.0% (titration)), polyvinylpyrrolidone (Sigma Aldrich, Cas Number 9003-39-8, PVP10), sodium chloride (Merck IC Standard, 1.19897.0500), and deionized (DI) water were used for all experiments. Pods of *Abelmoschus esculentus L.* (Certified by Biosystematics and Molecular Laboratory, Herbarium Padjadjaran University), Spectrophotometer Uv-Vis (Thermo Scientific, Multiskan Ex). Scanning electron microscope (Bronchure, SU3500), transmission electron microscope (Hitachi TEM System, HT7800), particle size analyzer (Horiba Scientific, SZ-100), zeta potential (Horiba Scientific, SZ-100), FITC annexin V (Invitrogen, USA, 25 mM HEPES, 140 mM NaCl, 1 mM EDTA, pH 7.4, 0.1% bovine serum albumin), Propidium iodide (Invitrogen, USA, 1 mg/mL PI (1.5 mM) solution in deionized water), Annexin-binding buffer (Invitrogen, USA, 50 mM HEPES, 700 mM NaCl, 12.5 mM CaCl2, pH 7.4), Medium RPMI-1640 (Merck, R0883), Fetal Bovine Serum (Merck, 12106C), Trypsin EDTA 0,05% (Merck, T4049), Phosphate Buffer Saline (Merck, P2272, pH 7,2), MTT assay (Merck, No.114650007001),. Lastly, Microscope (Olympus), Spectrophotometer Uv-Vis (Thermo Scientific, Multiskas Ex), Flow cytometer (BD FACSLyric™).

2.2. Preparation of Okra Raw Polysaccharide Extract (ORPE)

Okra pods were sourced from the Bandung traditional market in Indonesia with determination by Padjadjaran University. Fresh okra pods (500 g) were cut into pieces, mashed, and mixed with 500 milliliters of distilled water every night for three times. The supernatant was collected and centrifuged for five minutes at 4300 rpm. Next, the supernatant was precipitated in absolute ethanol for one time the sample volume, and the sample was incubated for twenty-four hours at 40^0C. The pellet was dissolved in distilled water and centrifuged. The supernatant was collected and lyophilized. This raw polysaccharide powder from okra fruit is called Okra Raw Polysaccharide Extract (ORPE) [11, 21].

2.3. Synthesis of AgNP-ORPE

Nanoparticle synthesis was conducted based on Tollen's method. ORPE, which contains polysaccharides, was used as a reducing agent to reduce the Tollens reagent $[Ag(NH_3)_2]^+$ (aq) into AgNPs. In addition to the prepared ORPE extract, mother liquor of $AgNO_3$ (10^{-3} M), sodium hydroxide (1.25×10^{-2} M), and PVP (8.4×10^{-5} M) were prepared. 12.5 mL of $AgNO_3$ was placed in an Erlenmeyer flask with a magnetic stirrer and agitated at 600–700 rpm to create the AgNP dispersion. Next, 12.5 mL of PVP mother liquor was added, one drop at a time, after 38.5 μL of ammonia solution. Lastly, using an automatic dosing syringe, 25 mL of 1:1 ORPE: NaOH was introduced and gradually homogenized at a rate of 75 mL/hour. Excess Ag^+, PVP, and ORPE were removed by ultracentrifugation at 12,000 G and filtered using a 0.1 μm filter membrane. AgNP-ORPE black powder of 0.1×10^{-2} mg was obtained and stored at 40°C. Furthermore, Faraday-Tyndall effect testing was carried out using laser light as an initial verification stage for the formation of AgNP-ORPE [22, 23].

2.4. AgNP-ORPE characterization

Optical characterization of AgNP-ORPE was performed using UV-Vis absorption spectroscopy. Nanoparticle size and surface tension were measured using a particle size analyzer (Horiba Scientific, SZ-100) at 25^0C with a detection angle of 90^0. Morphological analysis of the surface of biosynthesized silver nanoparticles (AgNPs) was performed using a scanning electron microscope at 30.000–100.000x magnification. Meanwhile, the remaining unused nanoparticle biosynthesis was deposited into 0.9% saline for further characterization using a Transmission Electron Microscope at 100.000-120.000x magnification to visualize the smallest structure of the formed silver nanoparticles. The stability of the AgNP-ORPE formed was inferred by zeta potential measurement [26].

2.5. Colon cancer cell viability and toxicity test

The MTT assay was used to assess the cytotoxicity of AgNP-ORPE. At a density of 1 x 10^4 cells/well, HCT 116 colon cancer cells were plated into 96-well plates. For 24 and 48 hours, cells were exposed to 1-100 μg/mL of AgNP-ORPE. MTT was then applied to each well, and the wells were incubated for four hours. Two hundred μL/well of DMSO was used in place of the extract and MTT combination. At 550 nm, the absorbance value was determined [27].

2.6. Assessment of the apoptotic potential

Apoptosis by trypsinization. In accordance with the well plate's arrangement, media and samples were taken from each well and placed into a marked centrifugation tube. One sterile PBS rinse was applied to the solution. PBS was gathered and returned to the appropriate tubes. 500 μL of trypsin 0.05% was applied to each well, and the wells were then incubated for five minutes at 37°C and 5% CO_2. One milliliter of complete medium was added to each well in order to halt the trypsin process. The cell suspensions were moved into the appropriate tubes from the wells. After being treated with AgNP-ORPE, colon cancer cells were stained for 20 minutes at room temperature using Annexin V-FITC and propidium iodide (PI). Flow cytometry was then used to analyze the cells that had undergone necrosis and apoptosis [28].

2.7. Colon Cancer Cell Cycle Analysis

One conical was prepared for each concentration of AgNP-ORPE. A total of 1 mL of media taken from the well was put into the transfer conical, and then 500 μL of PBS was added to each well. A total of 200 μL of 0.25% trypsin-EDTA was added and then incubated for 3 minutes. Resuspension was carried out so that the cells separated one by one by being observed under a microscope. After separating, it was then put into the conical. 500 μL of 70% alcohol was dripped 1 drop/second into the conical, which was gently shaken, and then the conical was kept at 40°C for 2 hours. Alcohol was discarded by centrifugation and then washed with PBS twice. The suspension was added to 25 μL PI (50x), 1 μL Rnase, and 0.5 μL Triton-X, and then PBS was added to 500 μL and then incubated for 30 minutes. The suspension was transferred into a FACS tube and then examined with a FACS Lyric flow cytometer to determine the cell cycle profile. Detection was performed on 10,000 cells [29].

2.8. Statistical Analysis

This study uses primary data from toxicity tests, cell viability tests, apoptosis evaluation, and cell cycle analysis to derive conclusions on the impact of AgNP-ORPE on the HCT 116 cell line, utilizing the Constant Variance Test statistics on the sigma plot to ascertain the significance of the AgNP-ORPE impact. Observation and descriptive data processing in terms of changes in electromagnetic wave light absorption were used to determine the status of cell alterations. All research findings are based on facts and are displayed as data, graphs, images, and the outcomes of statistical tests.

3. Result and Disscussion

3.1. AgNP-ORPE Synthesis Results

Polysaccharide extract from okra plant pods, or ORPE (Okra Raw Polysaccharide Extract), was obtained as much as 10.8 grams in the form of a slightly yellowish-white powder. This powder gives a distinctive aroma of the okra plant. Furthermore, this extract powder was used as a bioreductor to make nanosilver using Tollen's method. Moreover, a colorless reaction is produced during the synthesis of AgNP-ORPE created by Tollen's modification. According to Krishna Gudikandula and Singara Charya Maringanti's research, AgNPs can be produced biologically utilizing the white rot fungus *Pycnoporus* sp., which is 18–26 nm in size and has antibacterial properties [30]. AgNPs as large as 45 ± 2 nm (OLE) and 38 ± 3 nm (RLE) were produced by Muna A. Abu Dalo et al. in 2019, who modified the Tollens method with phytochemical olive leaf extracts (OLEs) and rosemary leaf extracts (RLEs) [23]. The Okra Raw Polysaccharide Extract (ORPE) Turkevich method was used by Kafesa et al. in 2023 to synthesize AgNPs, which had an average size of 285.1 nm. The characteristics of the resultant nanoparticles are typically color or color change [21].

The AgNP-ORPE produced due to the synthesis did not add color. Thus, irradiation with infrared light (Figure 1) was performed to ascertain the presence of the plasmon effect [31] (Faraday-Tyndall) to demonstrate the indication of the production of silver nanoparticles [26].
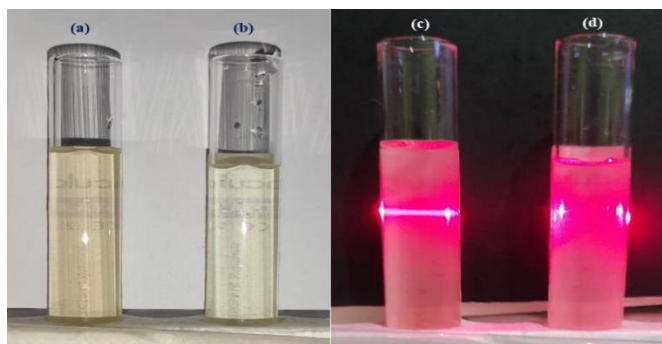

Figure 1.
Faraday-Tyndall (Plasmon resonance) effect of AgNP-ORPE. Solution without irradiation: (a) AgNP-ORPE, (b) Aquadest; and Solution with irradiation: (c) AgNP-ORPE and (d) Aquades.

Figure 1. a The AgNP-ORPE formed has a low volume fraction of nanoparticles due to the influence of other particle oscillations, resulting in no color formation. Additionally, the concentrations of AgNO3, NH3 precursor, ORPE, and PVP are quite small, and the reaction time is short. Based on Mie's theory, which supports Maxwell's theory [32], the origin of the nanoparticle color change is caused by dipole-dipole interactions in the effective medium, created by electromagnetic waves in the light field that induce surface polarization charges as a restoring force for free electrons [15, 16]. When electromagnetic waves in the form of laser light are applied, a plasmon resonance effect is formed (Figure 1.c). Ag+ has free electrons, where the frequency of the conduction electrons oscillates in response to the alternating electric field of the incident electromagnetic radiation. The oscillations that occur provide plasmon resonance in the visible spectrum. The oscillations are simple harmonic motion, described by the equation $X(t) = A \cos/\sin(\omega t + \Theta 0)$, where omega ($\omega$) is the angular frequency that visualizes the plasmon band effect [32]. When conditions are met, the maximum wavelength of absorption by AgNP-ORPE is condensed to a single surface plasmon band [33].

3.2. Characterization of AgNP Results

The confirmation of stability and characteristics of the AgNP-ORPE formed is supported by the UV absorption characteristics [33], with the appearance of absorbance peaks in the wavelength range of 200-300 nm (Figure 2). At UV and visible wavelengths, the $AgNO_3$ solution shows no absorption peak. Meanwhile, an absorbance spectrum was formed at a wavelength of 198.93 nm, indicating the formation of a new component in the form of AgNPs.
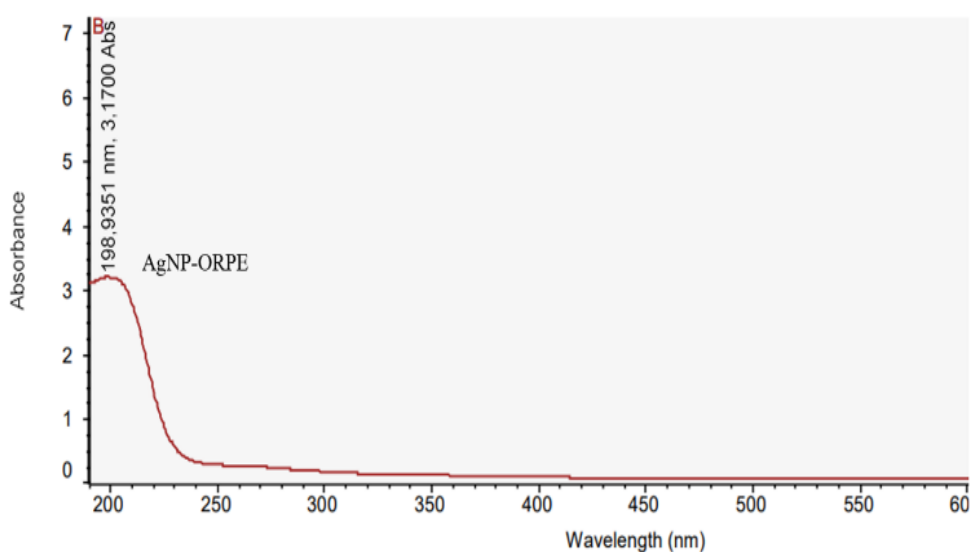

Figure 2.
UV spectrum of AgNP-ORPE.

After understanding the formation of AgNPs, their stability was determined based on the zeta potential value of -8.7 mV $\pm$ 0.15 mV at pH 9.1 (Figure 3). The dielectric constant becomes vulnerable to electrons in the outer shell of AgNP-ORPE, causing nonlinear optical properties at wavelengths around the plasmon resonance with large values and very fast(<1 ps) [33, 34]. This leads to the consequence and relaxation of the AgNP-ORPE electron distribution being unbalanced, which affects the zeta potential value of AgNP-ORPE. The zeta potential is a very good index of the magnitude of the interaction between colloidal particles [31, 34]. Based on the DLVO theory, the stability of a colloidal system is determined by the sum of van der Waals forces (ϕA) and electric double layer repulsive forces (ϕR) that exist between particles when close together due to Brownian motion [24].
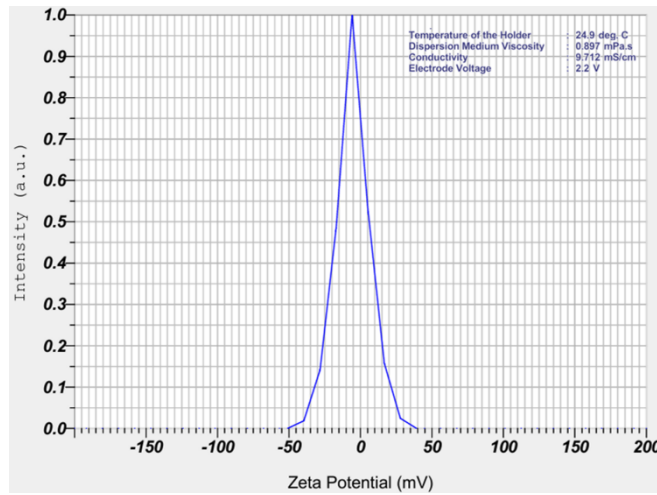
Figure 3.
Zeta potential of AgNP-ORPE.

Ag^+ has excellent solubility in water and leaves a negative surface charge that affects the distribution of ions at the interface and increases the concentration of the opposing ions to form an electrical double layer [35]. This modification of the Tollens' method to produce AgNP-ORPE with a pH of 9.1 has moderate stability. The zeta potential value of -8.7 mV ± 0.15 mV is close to the isoelectric point of the solution, so aggregation may occur, making the colloidal system not very stable [33, 35]. The impact of this instability causes particle agglomeration, where there is a slight collection and enlargement of particles when measured using a particle size analyzer with a mean particle size of 107.8 ± 25.47 nm and a polydispersity index (PDI) of 0.87521 ± 0.001 mPa.s (Figure 4).
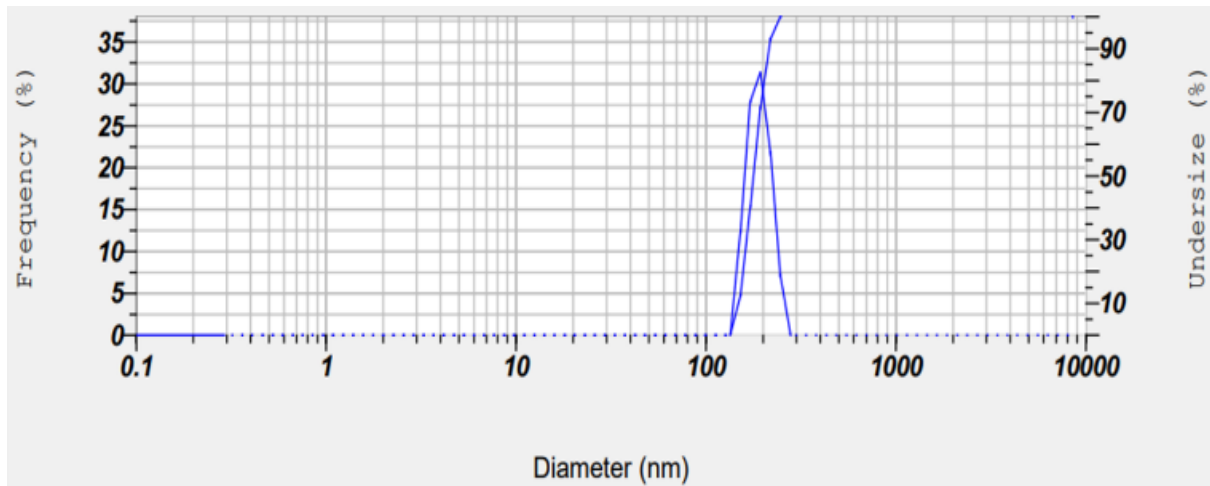

Figure 4.
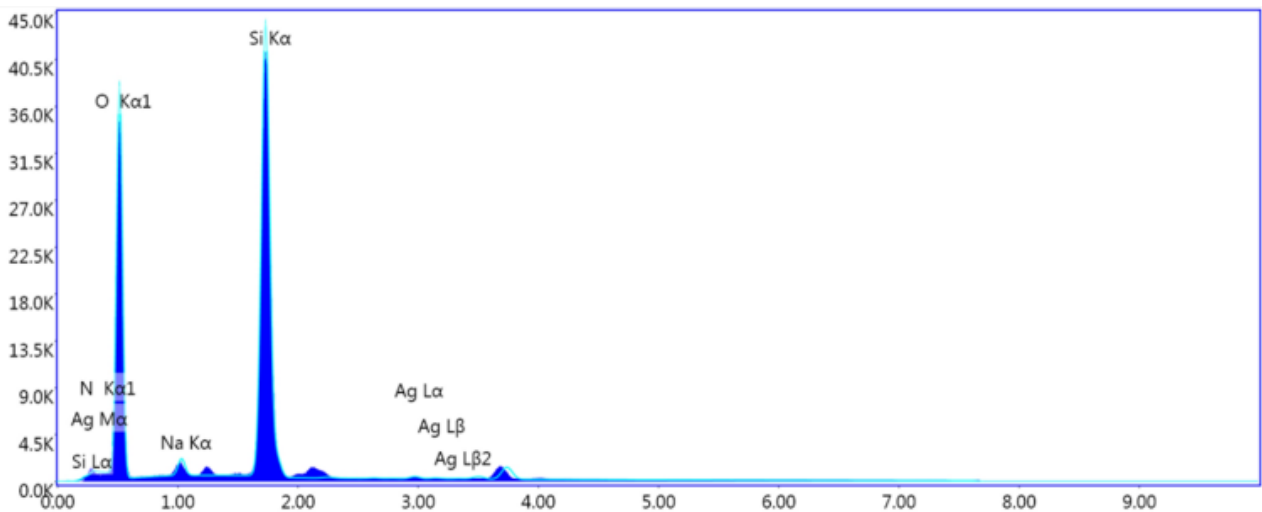Distribution particle of AgNP-ORPE by PSA.

Figure 5.
Energy-dispersive X-ray spectroscopy of AgNP-ORPE.

Because it contains solvent layers and surface coating materials affixed to the particle surface when it moves under the influence of Brownian motion, this PDI value should have a greater hydrodynamic diameter than the core [24, 36]. As illustrated in Figure 5, the AgNP-ORPE matrix revealed six constituent elements of AgNPs, with oxygen accounting for 64.94%, sodium for 2.07%, silica for 32.80%, and silver for 0.18% of the total. Since there aren't enough core electrons to be liberated to enable energy-dispersive X-ray spectroscopy emission [37] due to the low concentration of AgNP-ORPE, the energy produced by X-rays after striking the sample won't be sufficient to determine the proportion [34]. Furthermore, the monovalent ions in Ag+ have a relatively low electric double-layer pressure [35] which results in a tiny electric double-layer compression due to the small ion strength [33]. To establish steric hindrance that can adhere to the AgNP-ORPE surface and stop other particles from making close contact, PVP polymer is utilized to stabilize the colloidal system [24]. PVP is sufficiently distributed throughout the coating [38] to maintain the separation of AgNP-ORPE, which has an average size of 50–80 nm. The silver nanoparticles are anisotropic (ellipsoid) in shape when PVP is utilized as a protective barrier with Ag+ concentrations up to 0.02 M at low reaction temperatures and tiny concentrations (Figure 6).
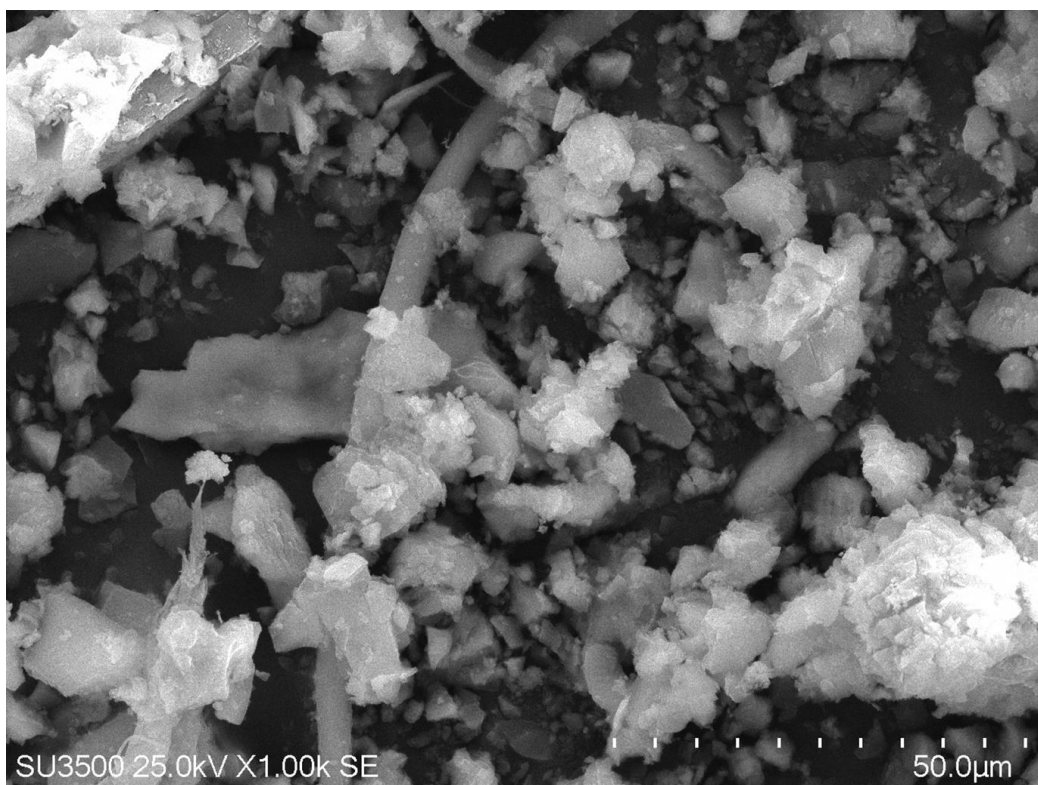

Figure 6.
SEM micrographs of AgNP-ORPE magnification 100.000x.

Gold is first applied to the produced AgNP-ORPE surface to enable electrical conduction upon the application of electrons [39]. Due to the solid condition of the measured material, SEM displays a great contrast. The signal from electrons interacting with the AgNPs' surface and then scattering back into an electron beam reflected by elastic scattering is picked up by the secondary electron detector [40]. Because there are more backscattered electrons [39] with higher energy than secondary electrons, the image appears brighter with a magnification of 100,000x, resulting in an increasingly distinct contrast (Figure 6). Even though they are still indistinguishable from one another, the asymmetrical circular shape of the AgNPs that are generated is more noticeable. AgNPs are distinguished by their apparent white/silver color [12]. Regardless of whether they are physically created or synthesized utilizing inorganic chemicals as catalysts [42]. AgNPs often feature spherical and/or octahedral geometries [41, 42]. The range of sizes and shapes found in this work is new and could serve special purposes in nanomedicine [43].

The constituent elements at a size of 500 nm influence the vivid black/white image that is produced by the SEM results in Figure 6. According to Ariani Edityaningrum et al. 2022, a constituent metal element with a higher atomic number will appear lighter or whiter than one with a lower atomic number [17]. The particles that have been found appear to be rounded and slightly aggregated.
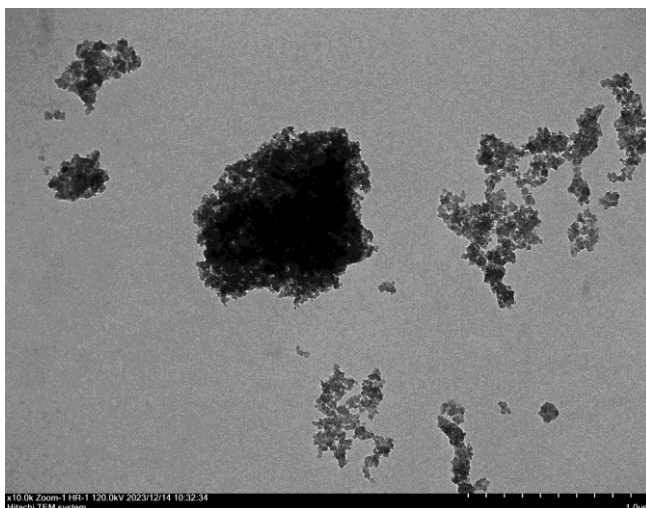
Figure 7.
TEM micrographs of AgNP-ORPE magnification 100.000x.

Figure 8.
TEM micrographs of AgNP-ORPE magnification 120.000x.

Figure 7 shows the findings of TEM investigations [44]. It is known that AgNP-ORPE made from anisotropic-shaped synthesis (ellipsoid) has an asymmetrical spherical appearance. It is evident that the AgNP-ORPE produced has a fairly high contrast [45] and that agglomeration causes distinct nanoparticle segregation [46]. The contrast decreases with decreasing AgNP size [47, 48]. Even though some sections of AgNP-ORPE are segmented, the shape cannot be determined since single nanoparticles with strong contrast do not yet emerge at a magnification of 100,000x (the particles still overlap).

The smallest size of AgNP-ORPE is 48.12 nm, with an average size of 50.85 nm (Figure 8). AgNP-ORPE exhibits a significant degree of curvature and appears to be combining into a single particle at a magnification of 120,000x. The resulting anisotropic spherical asymmetries shape is caused by the indentations that raise the confluence limit. The convexity criterion [44], which typically requires a minimum connectivity of 0.95, still applies to this geometry [45].

3.3. Colon Cancer Cell Viability and Toxicity Test

The AgNP-ORPE concentrations used in the toxicity test that calculates IC_{50} range from 2.5 to 100 µg/mL. As seen in Figure 1, the IC_{50} value provided varying reactions to the concentration and incubation duration that were established.
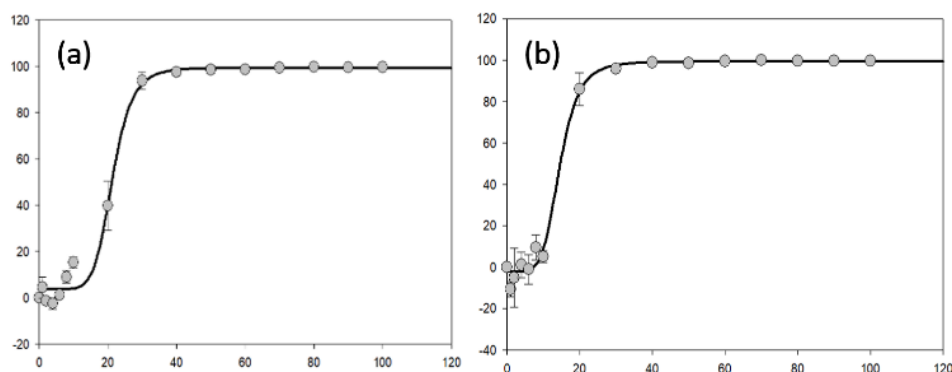
Figure 9.
Toxicity test (IC$_{50}$) of AgNP-ORPE against the HCT 116 cell line using SigmaPlot after incubation for 48 hours in RPMI-1640 media: (a) 24 hours of incubation, (b) 48 hours of incubation.

The IC$_{50}$ value of AgNP-ORPE after 24 hours of incubation at a concentration of 21.43 µg/mL and after 48 hours of incubation at a concentration of 14.64 µg/mL was calculated using a spectrophotometer and is displayed in Figure 9. This indicates that colon cancer cell lines may be killed by AgNP-ORPE. According to SigmaPlot's Constant Variance Test (Spearman Rank Correlation) (P = 0.0001), colon cancer cells dramatically die at higher AgNP-ORPE concentrations. As seen in Figure 10, the pattern of interaction between colon cancer cells and AgNP-ORPE is identical, indicating that the sample treatment is not affected by time, temperature, or humidity.
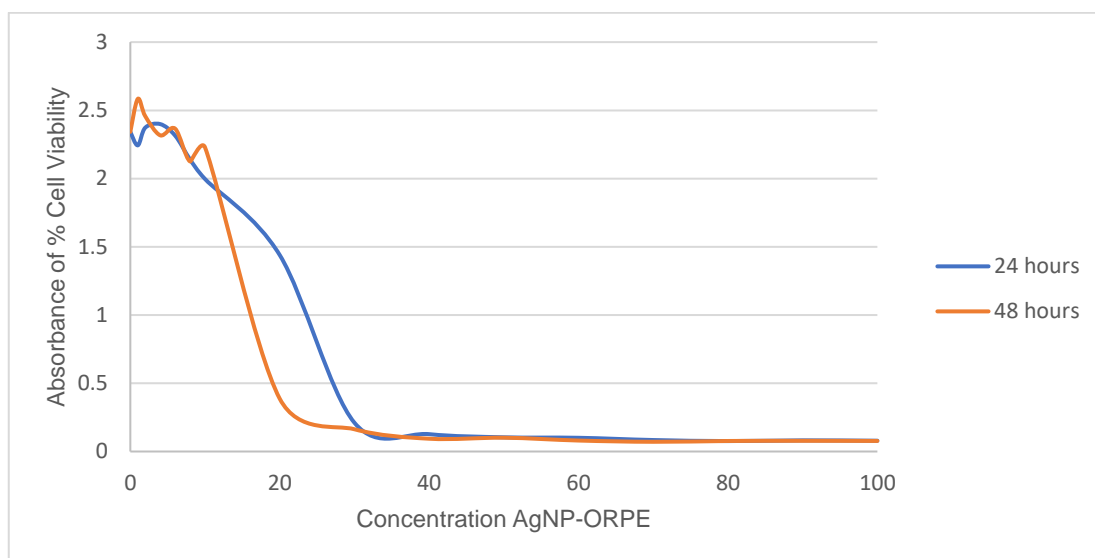

Figure 10.
Overlay dose response of cell viability HCT 116 human colon cancer cells with MTT assay with various concentrations of AgNP-ORPE 0,1 – 100 µg/mL incubated at 24 hours and 48 hours.

With each repetition, a decrease in the absorbance of the proportion of surviving cells may be observed at the dose of AgNP-ORPE given to HCT 116 cancer cells, as shown in Figure 10. Many cancer cells were still alive at AgNP-ORPE doses ranging from 0.1 to 30 µg/mL, according to the MTT staining experiment. The IC$_{50}$ sample concentration could not be ascertained after the cells were incubated for 24 hours since the 50% death requirement was not met by the cell death that transpired at a concentration of 21.43 µg/mL. Only a small number of dead cells were seen in the morphology of the colon cancer cells, which nevertheless contained living cells. Following a 48-hour incubation period, the absorbance of the treatment's proportion of surviving cells started to decline at a dose of 14.64 µg/mL, along with the appearance of nearly totally dead colon cancer cells. The ANOVA test, which is based on the above table, shows that the p-value for each incubation time has an average of >0.05. Calculations for inhibition were conducted under these conditions, and the IC$_{50}$ value was obtained at this concentration with a significant value at 24 hours (P=0.2217) and 48 hours (P=0.1984). Consequently, for both nanoparticle conditions at each different incubation temperature, the variance of the test choices is equivalent.

3.4. Apoptosis and Cell Cycle Analysis

AgNP-ORPE's morphological effect on the HCT 116 cell line was assessed by microscopically observing the sample treatment procedure [28, 49]. As observed in Figure 11, the media shows that the cell alterations are decreasing and that the lysed cell shape is nearly nonexistent.
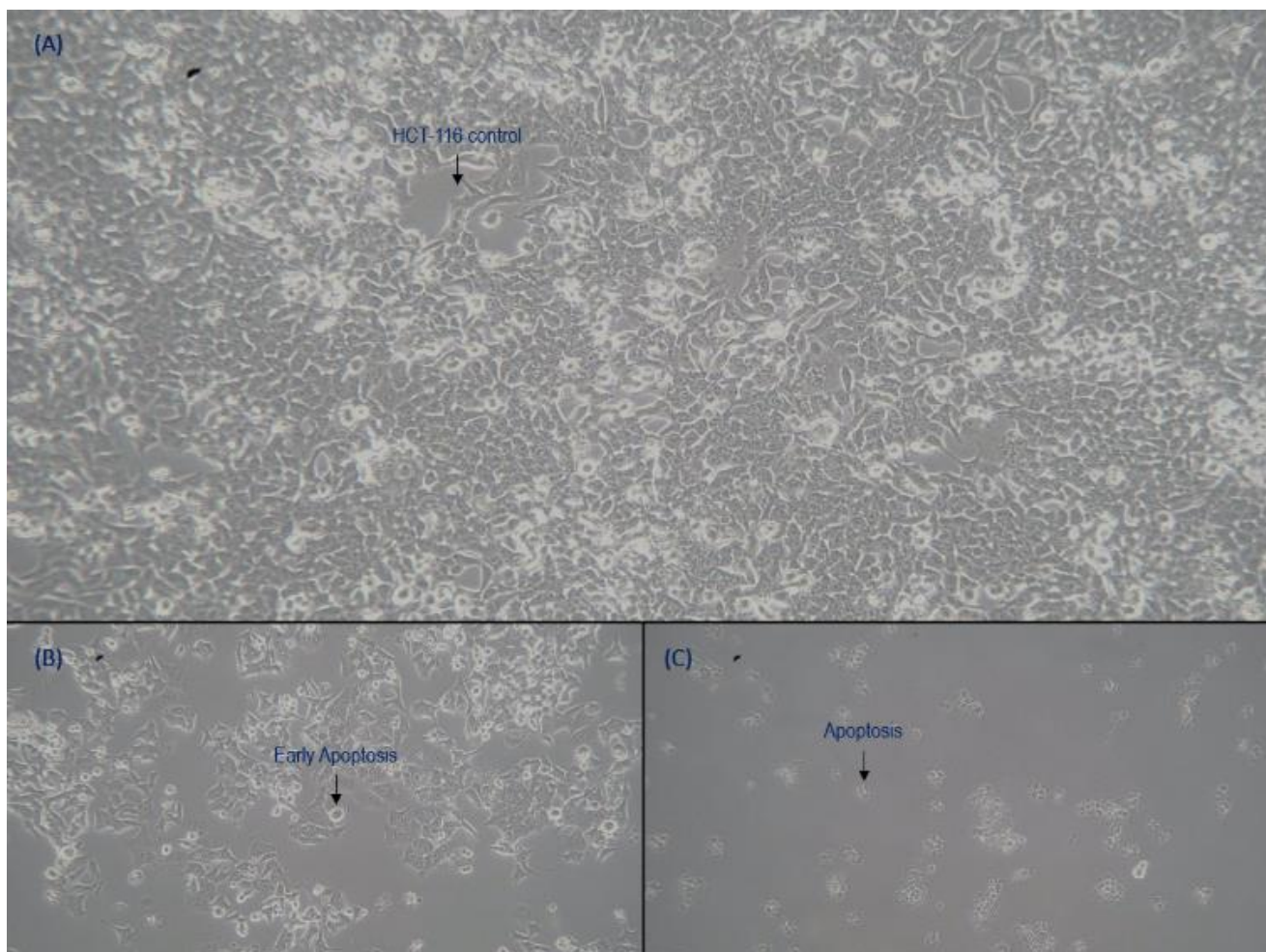
Figure 11.
Colon cancer cell line (HCT 116) changes during 48 hours of incubation in RPMI-1640 media: (a) 0 hours, (b) 24 hours, and (c) 48 hours.

Apoptotic cells exhibit distinct morphological and physical changes [50] such as cell shrinkage [51] and chromatin [52] and cytoplasm condensation [53] which can be quantified via flow cytometry or microscopic examination of the medium [54]. The release of cytochrome c via the development of channels linked to the Bax protein [55] and the mitochondrial permeability transition pore (PTP) also triggers apoptosis in the mitochondrial pathway [55, 56]. When released into the cytosol, cytochrome c will combine with ATP, caspase 9, and Apaf-1 to create an apoptosome complex [57]. Until the cell commits to apoptosis, these apoptosomes will trigger caspase-3 [58] which contributes to the cytoskeleton's disintegration and the cleavage of gelsolin, a protein that keeps cells morphologically stable [59].

Through the pores in the cell membrane, AgNP-ORPE particles smaller than 100 nm (50–80 nm) can simply diffuse through the colon cancer cell wall without the need for ATP [10]. AgNP-ORPE metal particles enter the cell and proceed to the mitochondria, where they catalyze the release of reactive oxygen species (ROS) by interacting with thiol groups and binding to the enzyme NADPH dehydrogenase (H2O2) [60]. Peroxiredoxin restricts ROS-related stimulatory effects on downstream targets of the mitogen cascade [61] and regulates H2O2 by relying on the thiol group being activated [62] and recruited to the receptor as part of the mitogenic process [63]. ROS are byproducts of metal-catalyzed oxidation or electron transport in mitochondria, which is aided by oxidoreductase enzymes [64]. To maintain the equilibrium between the generation and removal of ROS, ROS detoxification offers a cell defense mechanism [61, 63]. Cells undergo oxidative stress when there is an imbalance towards the pro-oxidative state [65]. According to Hu et al. [66] cells respond to stress by exiting the cell cycle and entering the G0 phase [66]. When cells are at rest, electrons from cytosolic NADPH can cross the membrane to molecular oxygen without NADPH activity, thanks to heterodimers of two polypeptides (p22-phox and gp91-phox) anchored in the membrane that also contain FAD groups [62, 66].

The mechanism of apoptosis will be activated by exposure to AgNP-ORPE or increasing ROS levels. Stress causes p21 to become active, which stops the colon cancer cell cycle from progressing [67, 68]. Furthermore, in response to oxidants, p53 and p27 cause retinoblastoma (pRB) to become dephosphorylated [27], which keeps cells in the S phase. The transcription factor Foxo, which is known to regulate the expression of genes involved in cell cycle development, partially regulates p27 expression [69]. Foxo3a is retained in the cell by mitogenic activation via the PI3K/Akt pathway, after which it penetrates the nucleus and enhances gene regulation for cell cycle termination [70].
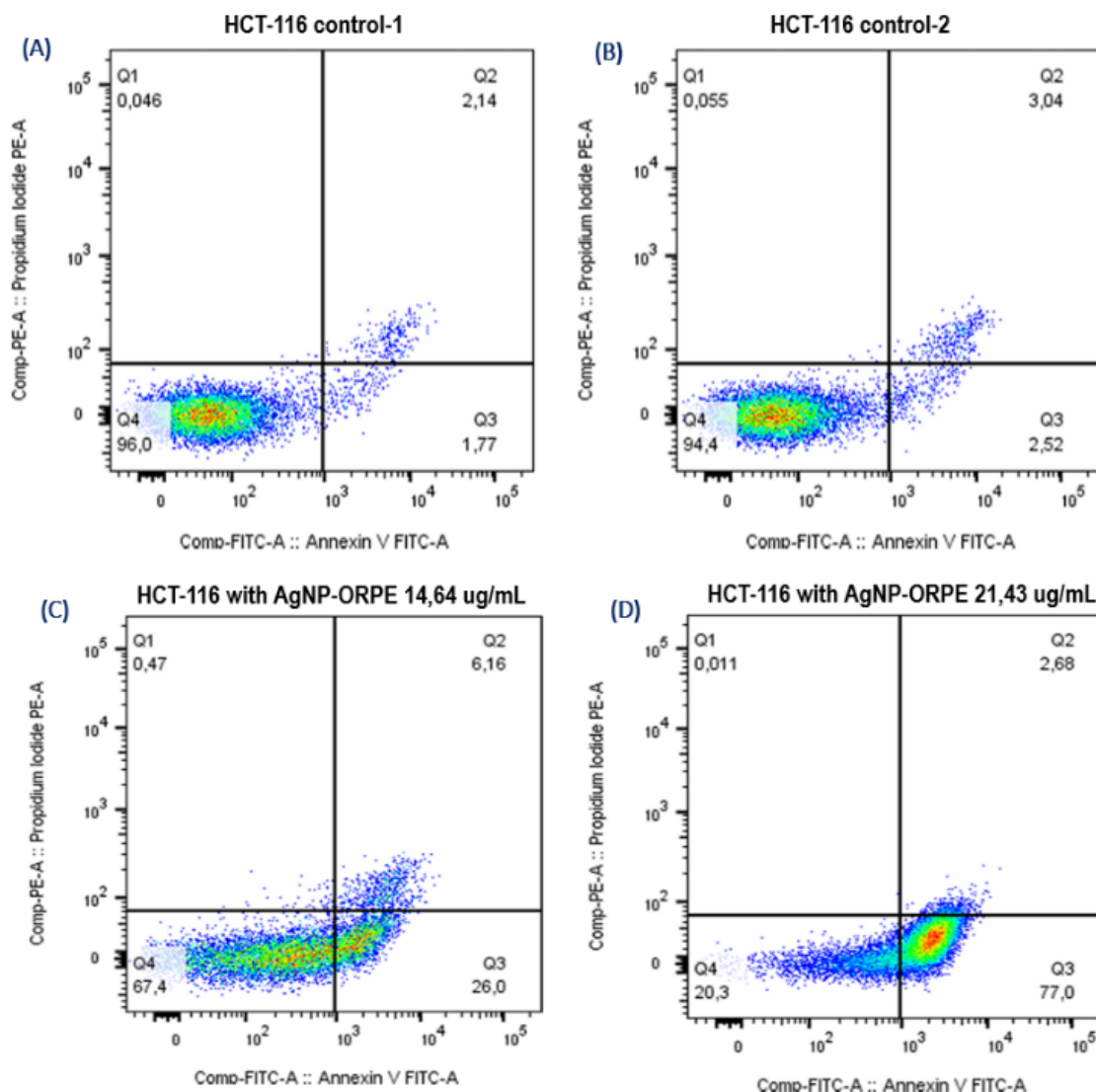
Figure 12.
Apoptosis analysis of HCT 116 cells using flow cytometry: (A) HCT-116 control-1, (B) HCT-116 control-2, (C) added AgNP-ORPE 14.64 μg/mL, and (D) added AgNP-ORPE 21.43 μg/mL.

The production of ATP and the cell's respiratory cycle are hampered by the interaction of these ROS produced in mitochondria with enzymes on the respiratory pathway [70]. With many restriction points (R), specifically G1/S, G2/M, and M, coordinated cell growth continues rigorously [6, 71]. The oxidative status of the cell influences the proteins and protein complexes that control each of these checkpoints [72]. Heintz and Burhans claim that oxidants regulate the departure from G0 and the arrival in G1 in response to external growth factors [73]. Cyclin D1 is an essential protein for reentry into the cell cycle, and its expression is driven by redox-dependent signaling pathways [72]. The cyclin D/CDK complex phosphorylates the primary regulatory site in G1 (retraction point = R) of the RB protein [74]. Furthermore, pRB phosphorylation has a redox potential of roughly -207 mV, at which point pRB cells become dephosphorylated and cease to circulate. For synchronized cells, Figure 5 illustrates that ROS generation rises with the cell cycle, peaking during the G2/M phase.

Table 1.
Cell cycle Phase cell line colon cancer HCT-116 with AgNP-ORPE.

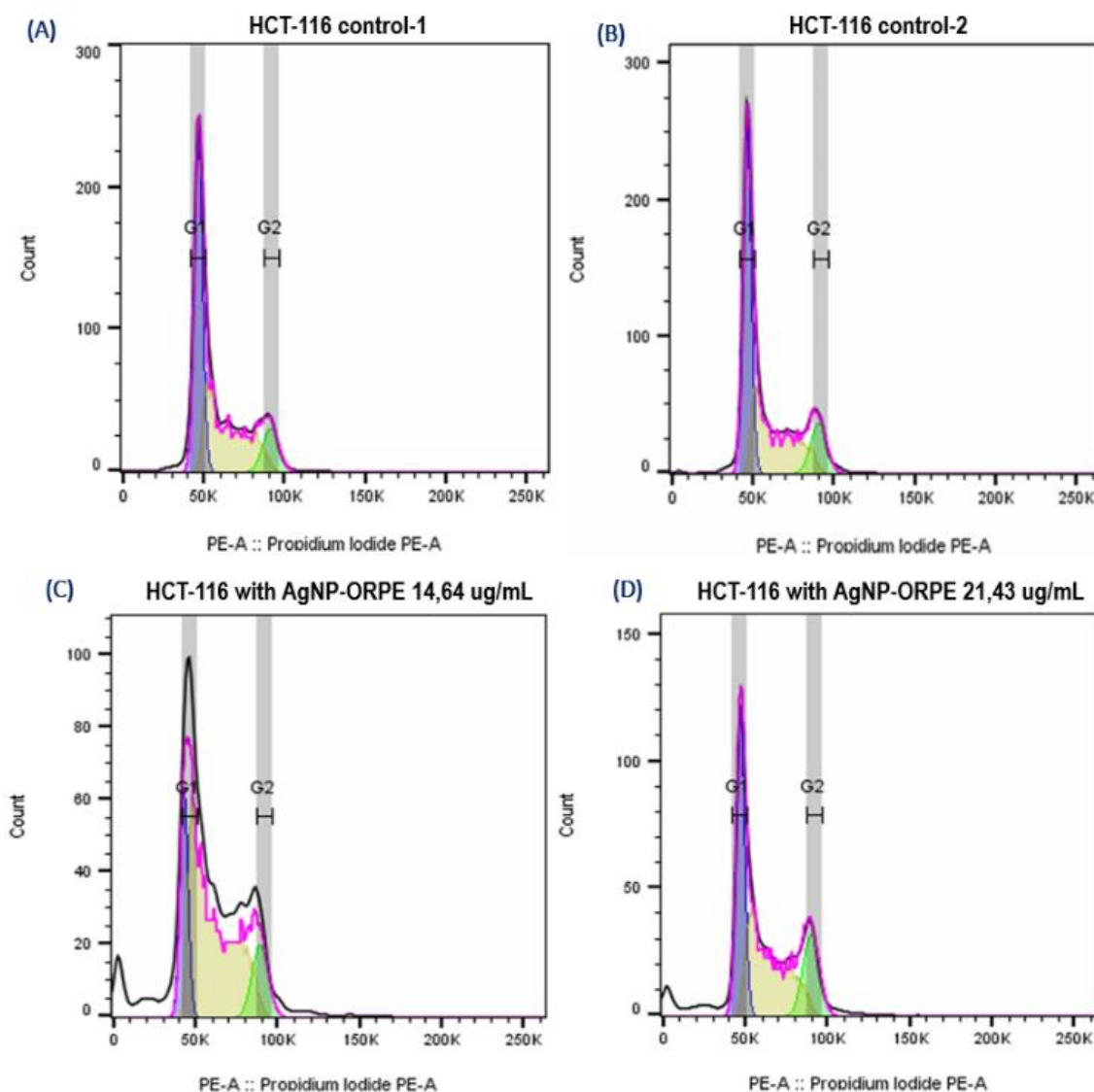| Phase	Control-1	Control-2	Concentration AgNP-ORPE	
			14.64 μg/mL	21.43 μg/mL
% G_1	43.4	46.2	17.2	32.7
% S	39.6	38.1	58.2	40.8
% G_2	10.7	12.7	11.0	16.3

Figure. 13.
Cell cycle analysis of HCT 116 using flowcytometri: (A) HCT-116 control-1, (B) HCT-116 control-2, (C) added AgNP-ORPE 14.64 μg/mL, and (D) added AgNP-ORPE 21.43 μg/mL.

As the cell cycle progresses, exponentially expanding cells undergo a number of modifications that can be identified by variations in the DNA content (DNA ploidy) [75]. Non-dividing normal (G0) or stationary (G1) diploid cells with DNA content are examples of asynchronous somatic cell populations [75, 76]. When AgNP-ORPE (Table 1) is added, the DNA content is inhibited (%G1 sample < %G1 control cells), preventing G1/S from continuing to the S phase at the site of retraction. If the DNA replicates in the S phase (synthesis), the cell's DNA content doubles (4N) and becomes tetraploid during the G2 and M phases, whereas cells in the S phase have a reasonable amount of DNA, specifically 2N and 4N [74-76]. Since DNA degradation is a characteristic of apoptosis, cell populations with DNA content below G0/G1 are seen in the sub G1 area and are recognized as apoptotic cells [77]. By using an internal standard to determine the location of the test sample's first peak, the ploidy level of G1 cells was determined. Diploid cells in G0/G1 have a total amount of DNA (2N) compared to tetraploid cells in G2/M (4N, with a 2-fold greater value), according to a DNA histogram produced by a flow cytometry study of the cell population derived from DNA. As a result, these stages can be distinguished by their distinct peaks. There is a zone between the G0/G1 and G2/M peaks, and DNA quantities between 2N and 4N are found on the sea surface. Cells at the G2-M transition phase can be bound by specific CDK1 inhibitors [74].

Other factors, such as cell type, medication, or treatment duration, may potentially influence the capacity of CDK1 inhibitors to cause G2 phase termination [75, 76]. Effective synchronization in specific cell types may therefore necessitate the optimization and validation of pharmacological treatment.

All things considered, these findings imply that AgNP-ORPE kills colon cancer cells by altering the permeability of the mitochondrial membrane and activating caspase. Compared to immunotherapy, the combination of chemotherapy and AgNP-ORPE particles has a positive impact on cancer treatment.

4. Conclusion

The new development of AgNP-ORPE production by Tollen's method produced anisotropic spherical asymmetries AgNPs with a size of 50.85 nm and good stability. It also had an anti-colon cancer effect by significantly reducing the proliferation of the colon cancer cell line HCT 116 in the G_0/G_1 phase and inducing apoptosis via the intrinsic pathway. Consequently, in conjunction with other therapeutic approaches, the potential of AgNP-ORPE for the treatment of patients with colon cancer can be thoroughly investigated.

References

[1]   C. Ni *et al.*, "Identification of octyl gallate, a novel apoptosis-inducing compound for colon cancer therapy, from Sanguisorba officinalis L. by cell membrane chromatography and UHPLC-(Q) TOF-MS/MS," *Heliyon,* vol. 10, no. 11, p. e32230, 2024. https://doi.org/10.1016/j.heliyon.2024.e32230

[2]   I. Mármol, C. Sánchez-de-Diego, A. Pradilla Dieste, E. Cerrada, and M. J. Rodriguez Yoldi, "Colorectal carcinoma: A general overview and future perspectives in colorectal cancer," *International Journal of Molecular Sciences,* vol. 18, no. 1, p. 197, 2017. https://doi.org/10.3390/ijms18010197

[3]   A. Y. Rompis and N. Dewi, "Genetic aspects of colorectal cancer," *Jurnal Sains dan Kesehatan,* vol. 2, no. 3, pp. 236-45, 2020. https://doi.org/10.25026/jsk.v2i3.145

[4]   D. Wu *et al.*, "Utilizing nanotechnology and advanced machine learning for early detection of gastric cancer surgery," *Environmental Research,* vol. 245, p. 117784, 2024. https://doi.org/10.1016/j.envres.2023.117784

[5]   L. B. Saltz, *Colorectal cancer: Evidence-based chemotherapy strategies*. New York: Springer, 2015.

[6]   C. Bellomo, L. Caja, and A. Moustakas, "Transforming growth factor β as regulator of cancer stemness and metastasis," *British Journal of Cancer,* vol. 115, no. 7, pp. 761-769, 2016. https://doi.org/10.1038/bjc.2016.255

[7]   S. Abdullah, S. Mukherjee, and B. Debnath, "The prevention of multi-drug resistance in cancers through the application of nanotechnology-based targeted delivery systems for combination therapies involving traditional Chinese medicine," *Pharmacological Research-Modern Chinese Medicine,* vol. 10, p. 100386, 2024. https://doi.org/10.1016/j.prmcm.2024.100386

[8]   L. Strużyńska, "Dual implications of nanosilver-induced autophagy: Nanotoxicity and anti-cancer effects," *International Journal of Molecular Sciences,* vol. 24, no. 20, p. 15386, 2023. https://doi.org/10.3390/ijms242015386

[9]   Y. Zhang, A. Rajput, N. Jin, and J. Wang, "Mechanisms of immunosuppression in colorectal cancer," *Cancers,* vol. 12, no. 12, p. 3850, 2020. https://doi.org/10.3390/cancers12123850

[10]   C. Yao *et al.*, "Gold nanoparticle mediated phototherapy for cancer," *Journal of Nanomaterials,* vol. 2016, no. 1, p. 5497136, 2016. https://doi.org/10.1155/2016/5497136

[11]   S. P. A. Wahyuningsih, M. Pramudya, I. P. Putri, D. Winarni, N. I. I. Savira, and W. Darmanto, "Crude polysaccharides from okra pods (Abelmoschus esculentus) grown in Indonesia enhance the immune response due to bacterial infection," *Advances in Pharmacological and Pharmaceutical Sciences,* vol. 2018, no. 1, p. 8505383, 2018. https://doi.org/10.1155/2018/8505383

[12]   P. Slepička, N. Slepičková Kasálková, J. Siegel, Z. Kolská, and V. Švorčík, "Methods of gold and silver nanoparticles preparation," *Materials,* vol. 13, no. 1, p. 1, 2019. https://doi.org/10.3390/ma13010001

[13]   M. Mitra, "Applications and properties of gold nanoparticles," *Nano Particle,* vol. 1, no. 1, pp. 1–10, 2019. https://doi.org/10.35702/nano.10004

[14]   R. Martien, A. Adhyatmika, I. D. Irianto, V. Farida, and D. P. Sari, "Development of nanoparticle technology as a drug delivery system," *Majalah Farmaseutik,* vol. 8, no. 1, pp. 133-144, 2012.

[15]   S. Iravani, H. Korbekandi, S. V. Mirmohammadi, and B. Zolfaghari, "Synthesis of silver nanoparticles: Chemical, physical and biological methods," *Research in Pharmaceutical Sciences,* vol. 9, no. 6, pp. 385-406, 2014. https://doi.org/10.4103/1735-5362.155514

[16]   T. Siddiqui, M. K. Zia, M. Muaz, H. Ahsan, and F. H. Khan, "Synthesis and characterization of silver nanoparticles (AgNPs) using chemico-physical methods," *Indonesian Journal of Chemical Analysis,* vol. 6, no. 2, pp. 124-132, 2023. https://doi.org/10.20885/ijca.vol6.iss2.art4

[17]   C. A. Edityaningrum, A. T. Oktafiani, L. Widiyastuti, and D. A. Arimurni, "Formulation and evaluation of silver nanoparticles Gel," *Journal of Pharmaceutical Science and Technology,* vol. 9, no. 2, pp. 125-138, 2022.

[18]   D. Ayers and A. Nasti, "Utilisation of nanoparticle technology in cancer chemoresistance," *Journal of Drug Delivery,* vol. 2012, no. 1, p. 265691, 2012. https://doi.org/10.1155/2012/265691

[19]   S. H. Lee and B.-H. Jun, "Silver nanoparticles: Synthesis and application for nanomedicine," *International Journal of Molecular Sciences,* vol. 20, no. 4, p. 865, 2019. https://doi.org/10.3390/ijms20040865

[20]   E. K. Sher *et al.*, "Nanotechnology in medicine revolutionizing drug delivery for cancer and viral infection treatments," *International Journal of Pharmaceutics,* p. 124345, 2024. https://doi.org/10.1016/j.ijpharm.2024.124345

[21]   A. Kafesa, W. Darmanto, and S. P. W. Wahyuningsih, "Silver nanoparticles with modified synthesis use sodium borohydride reducing agent and Okra (Abelmoschus Esculentus L.) raw polysaccharide extract as an anti-colon cancer," *Trends in Sciences,* vol. 21, no. 11, pp. 8149-8149, 2024. https://doi.org/10.48048/tis.2024.8149

[22]   A. Michalcová, L. Machado, I. Marek, M. Martinec, M. Sluková, and D. Vojtěch, "Properties of Ag nanoparticles prepared by modified Tollens' process with the use of different saccharide types," *Journal of Physics and Chemistry of Solids,* vol. 113, pp. 125-133, 2018. https://doi.org/10.1016/j.jpcs.2017.10.011

[23]   M. A. AbuDalo, I. R. Al-Mheidat, A. W. Al-Shurafat, C. Grinham, and V. Oyanedel-Craver, "Synthesis of silver nanoparticles using a modified Tollens' method in conjunction with phytochemicals and assessment of their antimicrobial activity," *PeerJ,* vol. 7, p. e6413, 2019. https://doi.org/10.7717/peerj.6413

[24]   C. G. Kolb, M. Lehmann, D. Kulmer, and M. F. Zaeh, "Modeling of the stability of water-based graphite dispersions using polyvinylpyrrolidone on the basis of the DLVO theory," *Heliyon,* vol. 8, no. 12, p. e11988, 2022. https://doi.org/10.1016/j.heliyon.2022.e11988

[25]   H. Ma *et al.*, "Polymer nanoparticle-based chemotherapy for spinal malignancies," *Journal of Nanomaterials,* vol. 2016, no. 1, p. 4754190, 2016. https://doi.org/10.1155/2016/4754190

[26]   A. Almatroudi, "Silver nanoparticles: Synthesis, characterisation and biomedical applications," *Open Life Sciences,* vol. 15, no. 1, pp. 819-839, 2020. https://doi.org/10.1515/biol-2020-0094

[27]   X. Wang *et al.*, "Sijunzi decoction enhances sensitivity of colon cancer cells to NK cell destruction by modulating P53 expression," *Journal of Ethnopharmacology,* vol. 329, p. 118115, 2024. https://doi.org/10.1016/j.jep.2024.118115

[28]   T. Gu *et al.*, "Intratumoural delivery of TRAIL mRNA induces colon cancer cell apoptosis," *Biomedicine & Pharmacotherapy,* vol. 174, p. 116603, 2024. https://doi.org/10.1016/j.biopha.2024.116603

[29]   G. Khalili-Tanha *et al.*, "Dual targeting of TGF-β and PD-L1 inhibits tumor growth in TGF-β/PD-L1-driven colorectal carcinoma," *Life Sciences,* 2024. https://doi.org/10.1016/j.lfs.2023.121865

[30]   K. Gudikandula and S. Charya Maringanti, "Synthesis of silver nanoparticles by chemical and biological methods and their antimicrobial properties," *Journal of Experimental Nanoscience,* vol. 11, no. 9, pp. 714-721, 2016. https://doi.org/10.1080/17458080.2016.1139196

[31]   N. El Biyari and M. Zekriti, "Advancements in surface plasmon resonance biosensors: A comprehensive review of technologies, applications, and future prospects," *Biotechnology Notes,* 2024. https://doi.org/10.1016/j.biotno.2024.11.002

[32]   M. R. Jalali, D. Kaushik, S. Verma, and H. Singh, "A coupled model of finite element method and Mie theory for heat transfer inside expanded perlite vacuum insulation panels (VIPs) at high temperatures," *International Journal of Heat and Mass Transfer,* vol. 219, p. 124885, 2024. https://doi.org/10.1016/j.ijheatmasstransfer.2023.124885

[33]   A. Demange and S. Fleutot, "Synthesis and characterization of a silver nanoparticle-based material," *Nanoparticle,* vol. 2, no. 1, pp. 1-5, 2020. https://doi.org/10.35702/nano.10005

[34]   M. Riswan, M. Arifin, I. Santoso, K. Nawa, K. Nakamura, and E. Suharyadi, "Effect of change in number of electrons to optical properties and surface plasmon resonance of noble metals," *Computational Materials Science,* vol. 247, p. 113519, 2025. https://doi.org/10.1016/j.commatsci.2024.113519

[35]   K. Jarzynska, A. Gajewicz-Skretna, K. Ciura, and T. Puzyn, "Predicting zeta potential of liposomes from their structure: A nano-QSPR model for DOPE, DC-Chol, DOTAP, and EPC formulations," *Computational and Structural Biotechnology Journal,* vol. 25, pp. 3-8, 2024. https://doi.org/10.1016/j.csbj.2024.01.012

[36]   F. S. Nejad *et al.*, "Investigating the effectiveness of iron nanoparticles synthesized by green synthesis method in chemoradiotherapy of colon cancer," *Heliyon,* vol. 10, no. 7, p. e28343, 2024. https://doi.org/10.1016/j.heliyon.2024.e28343

[37]   K. Ozaki *et al.*, "Hydrogen-bonded structure of hydrated water in polyvinyl pyrrolidone aqueous solution investigated by X-ray absorption and emission spectroscopy," *Journal of Molecular Liquids,* vol. 403, p. 124822, 2024. https://doi.org/10.1016/j.molliq.2024.124822

[38]   A. Abdelghany, N. Y. Elamin, S. Younis, and D. Ayaad, "Polyvinyl pyrrolidone/carboxymethyl cellulose (PVP/CMC) polymer composites containing CuO nanoparticles synthesized via laser ablation in liquids," *Journal of Molecular Liquids,* vol. 403, p. 124857, 2024. https://doi.org/10.1016/j.molliq.2024.124857

[39]   M. Hicks, K. Anamthawat-Jónsson, and Á. Einarsson, "The identification of bird eggshell by scanning electron microscopy," *Journal of Archaeological Science,* vol. 151, p. 105712, 2023. https://doi.org/10.1016/j.jas.2022.105712

[40]   A. Abdullah and A. Mohammed, "Scanning electron microscopy (SEM): A review," Retrieved: https://www.researchgate.net/publication/330169176. [Accessed 2019.

[41]   K. Mavani and M. Shah, "Synthesis of silver nanoparticles by using sodium borohydride as a reducing agent," *International Journal of Engineering Research & Technology,* vol. 2, no. 3, pp. 1-5, 2013. https://doi.org/10.13140/2.1.3116.8648

[42]   A. Pofelski, Y. Zhu, and G. Botton, "Relation between sampling, sensitivity and precision in strain mapping using the Geometric Phase Analysis method in Scanning Transmission Electron Microscopy," *Ultramicroscopy,* vol. 255, p. 113842, 2024. https://doi.org/10.1016/j.ultramic.2023.113842.

[43]   S. Wahab, M. Y. Alshahrani, M. F. Ahmad, and H. Abbas, "Current trends and future perspectives of nanomedicine for the management of colon cancer," *European Journal of Pharmacology,* vol. 910, p. 174464, 2021. https://doi.org/10.1016/j.ejphar.2021.174464

[44]   Y. Adachi, N. Yamamoto, and T. Sannomiya, "Focused light introduction into transmission electron microscope via parabolic mirror," *Ultramicroscopy,* vol. 251, p. 113759, 2023. https://doi.org/10.1016/j.ultramic.2023.113759

[45]   N. Gumbiowski, K. Loza, M. Heggen, and M. Epple, "Automated analysis of transmission electron micrographs of metallic nanoparticles by machine learning," *Nanoscale advances,* vol. 5, no. 8, pp. 2318-2326, 2023. https://doi.org/10.1016/j.ultramic.2023.113759

[46]   S. Meidaninikjeh, P. Mohammadi, and A. Elikaei, "A simplified method of bacteriophage preparation for transmission electron microscope," *Journal of Virological Methods,* vol. 328, p. 114951, 2024. https://doi.org/10.1016/j.jviromet.2024.114951

[47]   A. Engel, "Biological applications of the scanning transmission electron microscope," *Journal of Structural Biology,* vol. 214, no. 2, p. 107843, 2022. https://doi.org/10.1016/j.jsb.2022.107843

[48]   D. Den Engelsen, P. G. Harris, T. G. Ireland, G. R. Fern, and J. Silver, "Contrast and decay of cathodoluminescence from phosphor particles in a scanning electron microscope," *Ultramicroscopy,* vol. 157, pp. 27-34, 2015. https://doi.org/10.1016/j.ultramic.2015.05.009

[49]   D. Cruceriu, O. Baldasici, O. Balacescu, and I. Berindan-Neagoe, "The dual role of tumor necrosis factor-alpha (TNF-α) in breast cancer: molecular insights and therapeutic approaches," *Cellular Oncology,* vol. 43, pp. 1-18, 2020. https://doi.org/10.1007/s13402-019-00489-1

[50]   Q. Li *et al.*, "Structural characterisation and anti-colon cancer activity of an arabinogalactan RSA-1 from Raphani semen," *Carbohydrate Polymers,* vol. 342, p. 122417, 2024. https://doi.org/10.1016/j.carbpol.2024.122417

[51]   S. Khabbazian, E. Mirhadi, F. Gheybi, A. Askarizadeh, M. R. Jaafari, and S. H. Alavizadeh, "Liposomal delivery of organoselenium-cisplatin complex as a novel therapeutic approach for colon cancer therapy," *Colloids and Surfaces B: Biointerfaces,* vol. 242, p. 114085, 2024. https://doi.org/10.1016/j.colsurfb.2024.114085

[52]   N. Bhaskaran and L. Kumar, "Treating colon cancers with a non-conventional yet strategic approach: An overview of various nanoparticulate systems," *Journal of Controlled Release,* vol. 336, pp. 16-39, 2021. https://doi.org/10.1016/j.jconrel.2021.06.008

[53]   W. Ban *et al.*, "Boarding pyroptosis onto nanotechnology for cancer therapy," *Journal of Controlled Release,* vol. 370, pp. 653-676, 2024. https://doi.org/10.1016/j.jconrel.2024.05.014

[54]   E. Moghimipour and S. Handali, "Functionalized liposomes as a potential drug delivery systems for colon cancer treatment: A systematic review," *International Journal of Biological Macromolecules,* p. 132023, 2024. https://doi.org/10.1016/j.ijbiomac.2024.132023

[55] H. Khosravi, H. Manoochehri, A. Farmany, A. Khoshghadam, H. Rafieemehr, and R. Azmoonfar, "Bismuth selenide nanoparticles enhance radiation sensitivity in colon cancer cells in-vitro," *Biochemistry and Biophysics Reports,* vol. 38, p. 101732, 2024. https://doi.org/10.1016/j.bbrep.2024.101732

[56] P. Pandurangan *et al.*, "Integrating cutting-edge technologies: AI, IoT, blockchain and nanotechnology for enhanced diagnosis and treatment of colorectal cancer-A review," *Journal of Drug Delivery Science and Technology,* vol. 91, p. 105197, 2024. https://doi.org/10.1016/j.jddst.2023.105197

[57] S. A. Musthafa *et al.*, "Lectin isolated from Abelmoschus esculentus induces caspase mediated apoptosis in human U87 glioblastoma cell lines and modulates the expression of circadian clock genes," *Toxicon,* vol. 202, pp. 98-109, 2021. https://doi.org/10.1016/j.toxicon.2021.08.025

[58] S. Hayaza *et al.*, "Anticancer activity of okra raw polysaccharides extracts against human liver cancer cells," *Tropical Journal of Pharmaceutical Research,* vol. 18, no. 8, pp. 1667-1672, 2019. https://doi.org/10.4314/tjpr.v18i8.15

[59] S. Hayaza *et al.*, "Dual role of immunomodulation by crude polysaccharide from okra against carcinogenic liver injury in mice," *Heliyon,* vol. 7, no. 2, p. e06183, 2021. https://doi.org/10.1016/j.heliyon.2021.e06183

[60] I. M. De Rosa, J. M. Kenny, D. Puglia, C. Santulli, and F. Sarasini, "Morphological, thermal and mechanical characterization of okra (Abelmoschus esculentus) fibres as potential reinforcement in polymer composites," *Composites Science and Technology,* vol. 70, no. 1, pp. 116-122, 2010. https://doi.org/10.1016/j.compscitech.2009.09.013

[61] K. Khan *et al.*, "Mitochondria-derived reactive oxygen species are the likely primary trigger of mitochondrial retrograde signaling in Arabidopsis," *Current Biology,* vol. 34, no. 2, pp. 327-342. e4, 2024. https://doi.org/10.1016/j.cub.2023.12.005

[62] J. K. Kim and E.-K. Jo, "Host and microbial regulation of mitochondrial reactive oxygen species during mycobacterial infections," *Mitochondrion,* vol. 75, p. 101852, 2024. https://doi.org/10.1016/j.mito.2024.101852

[63] S. Nikseresht and A. Ahmadiani, "Investigating the insulin effects on nigrostriatal neurons survival and mitochondrial function in a rat model of Parkinson's disease. ResearchGate," Retrieved: https://www.researchgate.net/publication/318864620, 2017.

[64] F. Queenie *et al.*, "Shrinking the battlefield in cancer therapy: Nanotechnology against cancer stem cells," *https://doi.org/10.1016/j.ejps.2023.106586.,* vol. 191, p. 106586, 2023.

[65] Y. Gong and Y. Liu, "R-loops at chromosome ends: from formation, regulation, and cellular consequence," *Cancers,* vol. 15, no. 7, p. 2178, 2023. https://doi.org/10.3390/cancers15072178

[66] L. Hu *et al.*, "Glucose-6-phosphate dehydrogenase alleviates epileptic seizures by repressing reactive oxygen species production to promote signal transducer and activator of transcription 1-mediated N-methyl-d-aspartic acid receptors inhibition," *Redox Biology,* vol. 74, p. 103236, 2024. https://doi.org/10.1016/j.redox.2024.103236

[67] S. Ghazal, N. Khandannasab, H. A. Hosseini, Z. Sabouri, A. Rangrazi, and M. Darroudi, "Green synthesis of copper-doped nickel oxide nanoparticles using okra plant extract for the evaluation of their cytotoxicity and photocatalytic properties," *Ceramics International,* vol. 47, no. 19, pp. 27165-27176, 2021. https://doi.org/10.1016/j.ceramint.2021.06.135

[68] Y.-G. Yuan, S. Zhang, J.-Y. Hwang, and I.-K. Kong, "Silver nanoparticles potentiates cytotoxicity and apoptotic potential of camptothecin in human cervical cancer cells," *Oxidative Medicine and Cellular Longevity,* vol. 2018, no. 1, p. 6121328, 2018. https://doi.org/10.1155/2018/6121328

[69] J. Lun *et al.*, "Circular RNA circHIPK2 inhibits colon cancer cells through miR-373-3p/RGMA axis," *Cancer Letters,* vol. 593, p. 216957, 2024. https://doi.org/10.1016/j.canlet.2024.216957

[70] O. O. Ojo, O. G. Owajoba, A. B. Ojo, and O. A. Ojo, "Studies on melatonin intervention in reactive oxygen species-linked autophagy of neocarzinostatin-induced varicocele infertility in male Swiss Albino mice," *Phytomedicine Plus,* vol. 4, no. 3, p. 100595, 2024. https://doi.org/10.1016/j.phyplu.2024.100595

[71] J. Schröter *et al.*, "Generation of an induced pluripotent stem cell line (DHMCi009-A) from an individual with TUBB2A tubulinopathy," *Stem Cell Research,* vol. 64, p. 102879, 2022. https://doi.org/10.1016/j.scr.2022.102879

[72] C. Xu *et al.*, "Discovery and validation of a 10-gene predictive signature for response to adjuvant chemotherapy in stage II and III colon cancer," *Cell Reports Medicine,* vol. 5, no. 8, p. 101661, 2024. https://doi.org/10.1016/j.xcrm.2024.101661

[73] L. Krishnamurti, D. Ross, N. Bakshi, K. Khemani, C. Sinha, and G. Loewenstein, "Development, implementation, and testing of a web-based decision aid for facilitating shared decision making for disease-modifying therapies for sickle cell disease," *Blood,* vol. 128, no. 22, p. 5919, 2016. https://doi.org/10.1182/blood.v128.22.5919.5919

[74] T. Fauziah, R. R. Esyanti, K. Meitha, D. Hermawaty, and G. A. I. F. Wijayanti, "Cell cycle arrest via DNA Damage Response (DDR) pathway induced by extracellular self-DNA (esDNA) application in rice root," *Plant Physiology and Biochemistry,* vol. 219, p. 109370, 2025. https://doi.org/10.1016/j.plaphy.2024.109370

[75] J. Fahrer and M. Christmann, "DNA alkylation damage by nitrosamines and relevant DNA repair pathways," *International Journal of Molecular Sciences,* vol. 24, no. 5, p. 4684, 2023. https://doi.org/10.3390/ijms24054684

[76] L. Ballisat *et al.*, "Simulation of cell cycle effects on DNA strand break induction due to α-particles," *Physica Medica,* vol. 129, p. 104871, 2025. https://doi.org/10.1016/j.ejmp.2024.104871

[77] X.-L. Sun, H.-X. Song, J.-H. Li, Y.-J. Liu, X.-Y. Wang, and L.-N. Zhang, "TOE1 deadenylase inhibits gastric cancer cell proliferation by regulating cell cycle progression," *Biochimica et Biophysica Acta (BBA)-General Subjects,* vol. 1869, no. 1, p. 130736, 2025. https://doi.org/10.1016/j.bbagen.2024.130736